

Contents

<i>Acknowledgements</i>	3
<i>List of Papers</i>	4
1 Introduction	5
1.1 Current Use of Targeted Radiotherapy in Clinical Practice	5
1.2 Motivations for This Project	6
2 Methods for Measuring Spatial Distributions of Radioactivity	9
2.1 Radionuclide Imaging	9
2.2 Autoradiography	15
2.2.1 Film	15
2.2.2 Storage Phosphor Technology	16
2.2.3 Digital Instruments for Autoradiography	17
3 Methods for Dose Calculations	19
3.1 Definitions	19
3.2 MIRL Formulation	19
3.3 Calculations with Dose Point Kernels	21
3.4 Monte Carlo Simulations	21
3.4.1 EGS	22
3.5 Radiobiological Models	24
3.5.1 Is the Mean Dose a Useful Quantity?	25
3.6 An Illustration of the Dose Point Kernel Method and Monte Carlo Simulation	26
4 Dosimetry in Trabecular Bones	31
4.1 The structure of trabecular bone.	31
4.2 Calculations of Dose in Trabecular Bone	33
5 Dosimetry with Alpha-Emitting Radioimmunoconjugates	36
6 Summary of Papers	41
6.1 Paper 1	41
6.2 Paper 2	41

6.3 Paper 3	42
6.4 Paper 4	42
<i>7 Discussion and Conclusions</i>	<i>44</i>
<i>8 Future Work</i>	<i>48</i>
<i>9 References</i>	<i>50</i>

Acknowledgements

First of all I must thank my supervisor Arne Skretting for his support, his ever-lasting optimism, and his large effort in helping me with this work. He has been a major source of ideas, and his help with the manuscripts has been invaluable. My thanks also go to my co-supervisors, Øyvind Bruland and Dag Rune Olsen, and my co-worker Ellen Aurlien, for useful discussions that has been very important for my work. Øyvind has given me important input from the clinical side, which has helped me to set my work in perspective. I wish to thank Sindre Hassfjell and Christina Søyland for their help, the exchange of ideas, and their sincere interest in how my work was developing.

I wish to express my gratitude to the people at the Department of Nuclear Medicine. Throughout these years, they have supplied a friendly atmosphere and many interesting and useful discussions. Especially I want to thank Therese Seierstad for her friendly support, her willingness to help, and for standing out sharing the office with me for several years.

I thank my parents for their encouragement and for helping me to see the positive aspects in difficult times.

Finally I want to thank my wife for her great support, patience and love. My family with our two children, Sigrid Marie and Øyvind, is my great inspiration.

List of Papers

Paper 1

Kvinnsland Y, Stokke T and Aurlien E 2001 Radioimmunotherapy with alpha-particle emitters: Microdosimetry of cells with a heterogeneous antigen expression and with various diameters of cells and nuclei. *Radiat. Res.* **155** 288-96

Paper 2

Kvinnsland Y, Skretting A and Bruland O S 2001 Radionuclide therapy with bone-seeking compounds: Monte Carlo calculations of dose-volume histograms for bone marrow in trabecular bone. *Phys. Med. Biol* **46** 1149-61

Paper 3

Kvinnsland Y and Skretting A 2000 Methods for separation of contributions from two radionuclides in autoradiography with a silicon strip detector. *Phys. Med. Biol.* **45** 1183-93

Paper 4

Kvinnsland Y, Bruland Ø, Moe L and Skretting A 2001 A method for measurements of the uptake patterns of two beta-emitting radionuclides in the same tissue section with a digital silicon detector: Application to a study of $^{89}\text{SrCl}_2$ and $^{153}\text{Sm-EDTMP}$ in dogs with spontaneous osteosarcoma, *Submitted for publication*

1 Introduction

External radiotherapy has become a very important treatment modality for cancer. With the development of modern technology, the incidence of normal tissue complications has been decreased, and at the same time, higher doses to tumours have become obtainable. However, there will always be situations where the anatomical location of the target makes it impossible to avoid radiation injury in normal organs. Other difficult situations occur with widespread disease or with poorly defined boundaries of the tumour.

For such reasons, a more intelligent way of treating cancer with radiation has been sought. What is needed is a method to position the radiation emitter within or on the target. Furthermore, the radiation should have a range suitable for the size of the target. The solution to these demands is what has become known as targeted radiotherapy.

The idea is to label a cancer-seeking agent, the missile, with a radioactive nuclide, the warhead. Ideally, this provides a means to position the radiator in the target volume. By carefully choosing the radionuclide, the cancer cells can be exposed to radiation of the appropriate quality and range.

1.1 Current Use of Targeted Radiotherapy in Clinical Practice

Among all the radioactive compounds used throughout the years, the greatest success has been the use of ^{131}I in the treatment of thyroid cancer. The capability of thyroid tissue and differentiated thyroid cancer to accumulate and retain circulating iodine makes this a very effective treatment. At the same time, very modest injury is done to normal tissue, as the accumulated amounts of radioactivity are low in other organs, and the particle range is short.

Radioiodine has two roles in treating thyroid cancer. After the thyroid gland has been removed by surgery, ^{131}I is administered to ablate residual thyroid activity. If metastases occur later on, the radionuclide can be used again to treat these. Although the capability of the metastases to accumulate iodine is not as good as for normal thyroid tissue, the treatment is still effective, as there is no normal thyroid tissue acting as a competitive target.

Treatment with ^{131}I represents the simplest form of targeted radiotherapy. A natural uptake mechanism is exploited where the radionuclide itself is the targeting agent. Another example of this is the treatment of skeletal metastases with ^{89}Sr . Strontium has no natural role in the human body, but when injected as SrCl_2 , it is incorporated in bone as a calcium analogue.

With this form of treatment, the radionuclide is not necessarily accumulated in the cancer cells. Skeletal metastases often excite an osteoblastic response, and thereby formation of bone in which calcium plays an important role. Strontium-89 emits β -particles with sufficiently high energy for targeting the cancer cells that initiated the formation of bone, and thereby an indirect effect is achieved.

As with all forms of targeting radiotherapy, the limiting factor with ^{89}Sr is bone marrow toxicity. Being a bone seeking radioactive pharmaceutical, ^{89}Sr constitutes a much larger problem than ^{131}I . To improve on this, other bone seeking radioactive compounds have been invented. While awaiting the results of trials examining the potential of other compounds, $^{153}\text{Sm-EDTMP}$ remains the most important alternative to ^{89}Sr .

Physically, there are two important differences between ^{89}Sr and ^{153}Sm . First, the mean energy of the latter is much lower than that of the former. This is believed to have a positive marrow sparing effect. Second, the half-life of ^{153}Sm is 46,3 hours compared to 50,5 days for ^{89}Sr .

Contrary to ^{131}I and ^{89}Sr , ^{153}Sm as such has no bone seeking abilities, so this nuclide has to be bound to a bone-seeking agent. The compound that has been found to be the most appropriate is ethylene diamine tetramethylene phosphonic acid (EDTMP). $^{153}\text{Sm-EDTMP}$ is chemically stable, and preferentially concentrates in skeletal metastases. Another example of a targeting compound that is not naturally occurring in the body is $^{131}\text{I-m-IBG}$. This compound is used for the treatment of tumours derived from the neural crest.

When the first monoclonal antibodies were developed in 1976, it was hoped that this would lead to the construction of what has been called “magic bullets”. However, it has been difficult to find antibodies that only bind to cancer cells. The best results obtained with radioimmunotargeting (RIT) have been obtained in B-cell lymphomas. Non-Hodgkin lymphomas have well-characterised differentiation antigens, and this type of cancer is highly radiosensitive.

For a review of the current status of radionuclide therapy, refer to Gaze (1996), Lewington (1996), Chatal and Hoefnagel (1999), and McEwan (2000).

1.2 Motivations for This Project

Most of the clinical trials concerning palliative or curative treatment with radioactive compounds are focused on finding a direct relationship between administered activity and biological effects. Included in biological effects are the impact on metastases and primary

tumours in terms of regression or delay of progression, relieve of bone pain, and effects on normal tissue with bone marrow suppression being the most important. The activity is given to the patient and the observations are made.

However, knowledge of the direct relationship between administered activity and biological effects is not sufficient if one wants to gain insight into the mechanisms behind the observed effects. From a physicist's point of view, the natural approach is to include an intermediate step in the analysis: The administered activity results in energy depositions in tumours and normal tissue, which *thereon* give the observed biological effects.

It is the author's opinion that more detailed studies will be of major importance for the progress of treatment with radionuclides. On one hand, there is the question on what properties a radiopharmaceutical should possess, both chemical and physical. To answer this question, we need to understand the effects of different types of radiation as well as the uptake patterns of the compound in different tissues. Some information can be gained by carrying out classical *in vitro* survival studies of exposed cells. However, the more complex situation with cells organised in an organ or tumour, can only be studied *in vivo*. If more detailed studies of the uptake of radiopharmaceuticals and the subsequent biological effects were available, this would allow for a more direct study of the radiobiology and the resulting impact on tumour size and organ functions.

To further increase the level of understanding, known distributions of radionuclides in the tissues must be converted into spatial dose distributions, or, even better, into microdosimetric probability distributions. The observed biological effects are a result of the stochastic pattern of energy deposition, and can not always be analysed solely in terms of the deterministic dose or, even worse, in terms of the mean organ dose. It is important to bear this in mind when effects of different radionuclides, emitting different types of radiation (for instance α -emitting nuclides and β -emitters), are compared.

Another aspect is related to the treatment planning. If one could predict the uptake pattern in a patient along with the resulting effects, before administrating the activity, the treatment with radionuclides could be adjusted for the individual patient. This should also be investigated for approaches where radionuclide treatment is considered adjunct to external radiation.

Information on the uptake pattern could be obtained in several ways. One could measure the uptake pattern of a tracer amount of the radiopharmaceutical, one could measure the uptake of a compound with equal chemical properties, or one could rely on empirical data that describe the relationships between various patient characteristics and uptake patterns.

Furthermore, to translate the predicted uptake into biological effects, basic understanding of the radiobiology has to be acquired.

The papers contained in this dissertation are concerned with topics at different stages of this path towards an understanding of the effects following administration of radioactive compounds. Paper 1 deals with the special problems of microdosimetry with alpha-emitting nuclides. Paper 2 addresses the problem of calculating dose distributions in trabecular bone with bone seeking radioactive compounds. In paper 3 and 4, methods are developed for the simultaneous measurement of the distributions of two radionuclides in one section of tissue. These methods may be used for a direct comparison of the uptake pattern of different radioactive compounds. In paper 4, the uptake patterns of ^{89}Sr and $^{153}\text{Sm-EDTMP}$ are compared in dogs with osteosarcomas, using one of these methods.

2 Methods for Measuring Spatial Distributions of Radioactivity

The first steps towards an understanding of the observed effects of targeted radiotherapy, are measurements of the uptake of radiopharmaceuticals. This is also crucial for monitoring ongoing treatment and for treatment planning. The mean dose to an organ is proportional to the *cumulated activity*, the number of decays taking place in the source organs, and therefore, an essential part of the research towards a new radiopharmaceutical is measurements of the pharmacokinetics (Strand et al 1993, Siegel et al 1999, Stabin 1999).

With humans, the only way of obtaining this information is radionuclide imaging. (Exceptions are measurements on drawn blood, urine, and faeces.). Because of limited spatial resolution, such information must be supplemented by measurements of the sub millimetre scale distribution in comparable animals and tumours. Autoradiography is therefore an important tool to obtain sufficiently detailed distribution data for estimation of absorbed radiation dose.

2.1 Radionuclide Imaging

Over the last decades, there has been a rapid technological development of instruments for radionuclide imaging (Links 1998). Today, mainly three methods are used for imaging of radionuclides in humans (Leichner et al 1993, Ott 1996): *planar scintigraphy*, *single photon emission computed tomography* (SPECT) and *positron emission tomography* (PET). SPECT and PET investigations provide tomographic (3-dimensional) information, while planar scintigraphy only gives 2-dimensional information. Involved in all these methods are one or several cameras that register photons emitted from the nuclides. This information is processed, and planar images or 3-dimensional matrices representing activity distributions, are found.

A *gamma camera*, used for planar scintigraphy and SPECT investigations, usually consists of a single scintillating crystal sandwiched between photomultipliers (PMT) and a lead *collimator* (Fig 2.1). Photons that enter the crystal may interact with the material, either by the Compton process or by the photoelectric process, and energy is transferred to electrons. As the released electrons are slowed down and their energy is deposited, electrons in the crystal are excited. When they return to their original state, this is accompanied by emission of

photons. These photons are picked up by the PMTs and an electrical pulse is created and sent to the electronics.

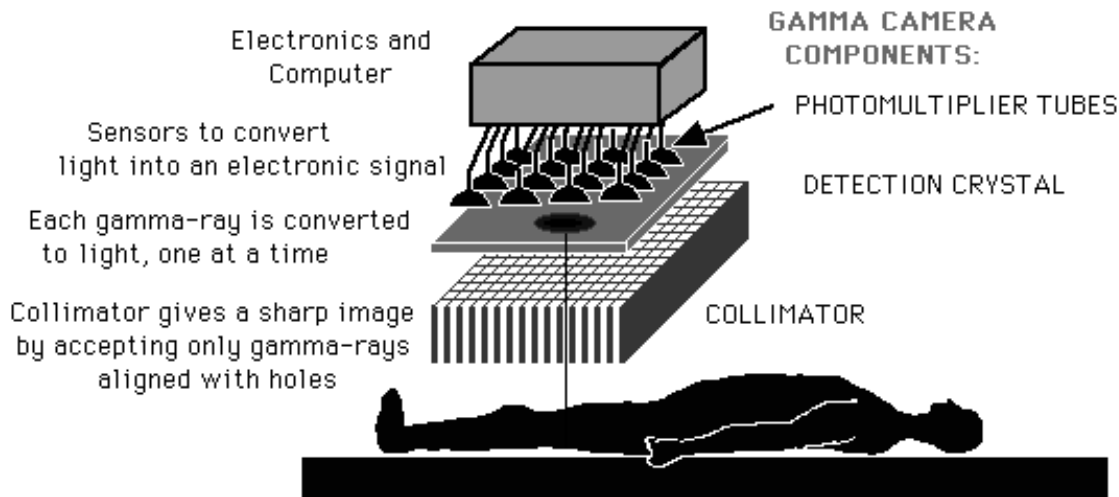


Figure 2.1 Schematic figure of a gamma camera.

The material and thickness of the crystal is optimised for specific energy intervals. In a gamma camera, the crystal usually is optimised for energies below 200keV, mainly because the majority of the examinations are performed with ^{99m}Tc , which emits photons of 140keV. The most widely used crystal in gamma cameras consists of sodium iodide (NaI) doped with small amounts of thallium. This is a well-suited material because of a high yield of photons, its low self-absorption of scintillation photons, and an acceptable decay time (The time it takes for a certain amount of the electrons to return to their original state.). A rapid decay is necessary for high count-rate acquisition.

When a photon hits the detector, the position of interaction in the detector is determined by the electronics, but this gives no information about the origin of the particle. The collimator acts to select the directions of the incoming photons, and to define the geometrical field of view. In a gamma camera, it usually consists of a block of lead with holes of a certain length and cross sectional area through which the photons may travel.

Independent of the type of collimator used, *scattered* photons will degrade the images. A photon that is emitted in a direction that is incompatible with detection may be scattered into a new direction that is accepted by the collimator. In the case where there is only a small

change in energy, the energy selection mechanism of the gamma camera cannot distinguish this photon from the unscattered photons.

With a parallel hole collimator, the intensity in a pixel is proportional to the activity in the volume of the subject that is covered by this pixel, *attenuated* by the mass located between the activity and the gamma camera:

$$I \propto \int_{x_1}^{x_2} A(x) \exp\left(-\int_x^{x_2} \mu(x') dx'\right) dx. \quad (2.1)$$

x_1 and x_2 are the distances between the camera and the posterior and anterior sides of the patient, and $\mu(x')$ is the linear attenuation coefficient. A planar scintigram is more or less the same thing as a photograph, the only difference being the energy of the photons.

With simultaneously acquired anterior and posterior images together with transmission data, an approximate calculation of the activity within some source region can be done using the *conjugate view* method. In the absence of attenuation, denoting the total intensities within the region of interest (ROI) in the anterior and posterior images by I_A and I_B , the activity is proportional to the square root of the product of these numbers:

$$A \propto \sqrt{I_A I_P}. \quad (2.2)$$

In order to find the absolute value of A , the product under the square root sign has to be multiplied with a factor equal to the attenuation through the body, and a factor accounting for the spatial extension of the source volume. For details about refinements of this method, refer to Siegel et al (1999).

In SPECT studies, many planar images are acquired at different angles relative to the object by letting the camera rotate around the object with the detector surface parallel to the rotation axis. These images may also be considered as projections of the 3-dimensional information onto many different planes. The projections are processed to reconstruct the 3-dimensional activity distribution. The simplest algorithm used for this purpose (explained in Swindell and Webb 1988) is *filtered back-projection*, illustrated in fig. 2.2. In the absence of attenuation and noise, this algorithm perfectly reproduces the source distribution.

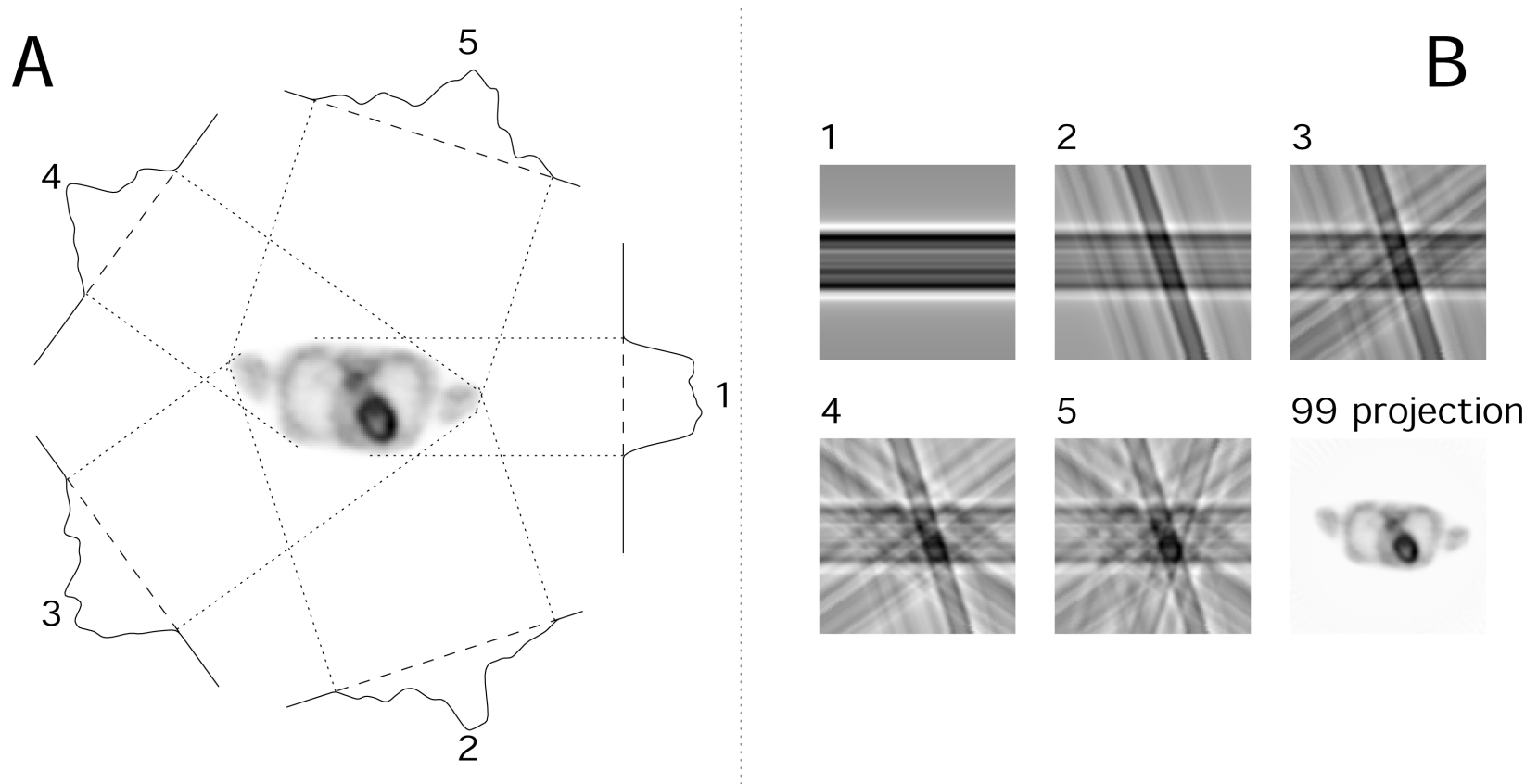


Figure 2.2 The principle of filtered back-projection. A: Projections of the activity distributions are measured with the camera. In this example five projections are measured. B: After a filter operation the projections are added into the reconstructed image. Images 1-5 show the reconstructed image after the inclusion of 1-5 projections, while the last image shows the result when 99 projections are used.

By offering 3-dimensional information, SPECT has a huge advantage over planar scintigraphy (Siegel et al 1999). With SPECT, it is possible to delineate 3-dimensional volumes and find the activity within that volume. Such procedures require, however, proper corrections for the effects of attenuation and scatter (Ljungberg and Strand 1990, Ljungberg and Strand 1991, Ljungberg et al 1994). Recently, iterative SPECT reconstruction methods have been developed that take effects of attenuation, scatter, and variation in resolution with distance into account (Floyd et al 1986, Kim et al 1992, Liang 1993). Especially when combined with CT- or MR-information, rather accurate estimates can be obtained for the specific activity.

In SPECT studies and planar scintigraphy, the distributions of radioactive nuclides are found by detecting single photons emitted by the nuclides when they decay. PET, positron emission tomography, is based on a different mechanism. Some nuclides emit positrons, the antiparticle of the electron. In the same way as with electrons, these are slowed down rather quickly and absorbed by the medium, so a direct detection of positrons is impossible. However, when a positron has come to rest or a small velocity, it annihilates together with an electron, and two photons are created. These photons travel in approximately opposite directions (Fig. 2.3).

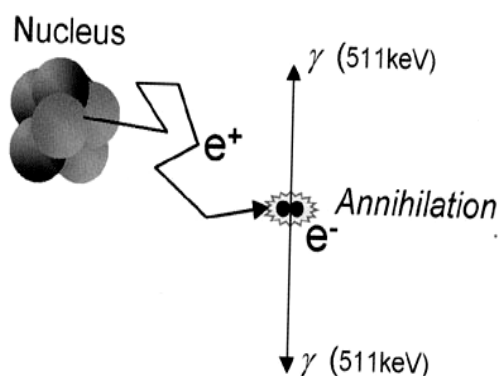


Figure 2.3. Emission of a positron and the subsequent annihilation.

If both these photons are registered together with their positions of detector interaction, one knows that the decay of the nuclide took place somewhere along the line connecting these positions. Physical collimation is unnecessary, and much higher detection efficiency is possible.

Most modern PET scanners consist of a barrel shaped device consisting of many detectors. A less effective, but probably adequate solution for many clinical purposes, is a

configuration consisting of two gamma cameras at opposite positions that rotate around the patient. An event is accepted if two hits occur within some time window and the deposited energies fall within selected windows.

The photons created in the annihilation have energies equivalent to the rest mass of an electron, and is equal to 511keV. This is considerably higher than the energy of the photons of for example ^{99m}Tc and ^{153}Sm (140keV and 103keV). This means that the detector has to be thicker, or have a higher density, to obtain a high detection efficiency. In modern PET machines, the most common detector material is BGO ($\text{Bi}_4\text{Ge}_3\text{O}_{12}$), which has a density that is approximately twice that of NaI (7,1 g/cm³ vs. 3,7 g/cm³).

A further advantage in PET compared to SPECT is in the reconstruction. When a positron and electron annihilates, two photons are emitted in opposite directions, and both photons have to be detected if a hit is to be recorded. This means that it is the total attenuation along the line of travel, through the entire body, that is of interest. One does not have to know the attenuation as a function of position in the body, and this largely simplifies the reconstruction algorithm. The necessary attenuation data are acquired by means of a point source for which the transmission is measured at all angles (transmission scan), but may also be derived from a set of CT-images.

A source of noise that is not present in SPECT or planar scintigraphy is what has become known as *random coincidences*. This occurs when two decays take place within a sufficiently short interval of time. Then two photons originating from two different positrons may be registered and interpreted as if the two photons came from the same positron. Obviously, this gives rise to errors in the reconstruction. This form of noise is the most difficult to deal with in PET because of its random nature.

The critical parameter is the length of the time window in which the registration of the two photons takes place. If this window can be made narrower, the probability of random coincidences is reduced. This can be accomplished with the introduction of new detector materials with shorter decay times. An example of such a material is LSO (Lu_2SO_5) which has a decay time that is 7,5 times shorter than that of BGO.

However, in total, a much better spatial resolution is obtained with PET than with SPECT (Siegel et al 1999). This has several consequences. With a small source volume, the volume into which the activity is reconstructed is smaller, giving a more correct specific activity and a better signal to noise ratio. This means that it is easier to detect elevated activity concentrations in small volumes. Furthermore, the position of an activity focus is better defined.

The increased sensitivity of PET can allow for an accurate pre-therapy dosimetry if a radioactive positron-emitting compound exists, that has equal chemical properties as the therapeutic compound (Lundqvist et al 1999, Lubberink et al 1999, Pentlow et al 1996). A small amount of this compound is given to the patient in advance of the therapy, the distribution of this activity is measured, and assuming the same distribution with the therapeutic activity, the dose calculations can be done. Alternatively, and possibly the best solution, the positron-emitting compound can be given together with the therapeutic compound, allowing for a direct measurement of the kinetics.

The latest achievement in detector technology is a combined PET and CT (Beyer et al 2000). This apparatus does a simultaneous measurement of activity and attenuation, which allows for a very accurate correlation of activities with anatomical structures. Furthermore, the attenuation data, necessary for reconstruction, are calculated from the CT-measurements with a conversion that takes the difference in photon energy into account, and a point source is no longer necessary for transmission scans.

2.2 Autoradiography

In spite of the improvement in geometrical resolution introduced by the PET technology, there is still a need for the capabilities of autoradiography. Intuitively, inhomogeneities over distances of the order of the particle ranges are of importance. The introduction of radionuclides emitting Auger-electrons or α -particles thus introduces the need for micrometer resolution in measurements of radionuclide distributions. This is far below the achievable resolution of PET.

Autoradiographic imaging modalities are capable of delivering this kind of resolution. However, only 2-dimensional information is directly available. Also, the image acquisition can only be done with tissue sections, and measurements with live objects are therefore impossible. For a detailed description of autoradiography techniques, see Upham and Englert (1998).

2.2.1 Film

Autoradiography has traditionally been performed with film. The technique is based on the reduction of silver ions in a film emulsion as a result of energy depositions by traversing β -particles. If localisation at the cellular or subcellular level is needed, the section must be

brought into direct contact with the emulsion. This is accomplished by emulsion dipping or by emulsion-coated cover slips that are brought into close contact with the sections. With less strict requirements on resolution, film is applicable.

For a certain exposure time, a lower activity threshold exists for a blackening of the film. Furthermore, with high activities, saturation occurs, and thus the linear dynamic range is limited. With most films, the linear dynamic range is 1,5-3 logs of activity. This limited range necessitates a good estimate of the exposure time in advance of the exposure to avoid underexposure or saturation.

For each quantitative measurement, calibration is necessary. This is accomplished using multiple standards with different activities, which are incorporated into each exposure. For each standard, the optical film density is measured, and a graph can be obtained which shows the relationship between activity and density.

The main advantage of film compared to other imaging modalities, is the very good resolution. With ^3H and ^{125}I , resolutions of 0,5-1,0 μm are possible. However, the laborious procedures with the calibration limit its usefulness for quantitative studies. Details of dosimetry with film are investigated in Yorke et al (1993), Humm et al (1993), Humm et al (1994), Humm et al (1995), Roberson et al (1992) and Muthuswamy et al (1996). In Humm et al (1995), Roberson et al (1995) and Muthuswamy et al (1996), the possibilities for combining autoradiographs of serial sections into a 3D activity distribution are explored.

2.2.2 Storage Phosphor Technology

A phosphor screen imaging system is composed of imaging plates, a laser, and a light detection system. The sample to be measured is placed on top of an imaging plate, which contains photostimulable crystals, BaFBr:Eu^{2+} . When ionising particles deposit their energy, electrons are brought into an excited state, and may be captured, still in excited states, in 'electron traps'. By exposing these crystals with red light (633nm), with a laser spot scanning the plate, the electrons are further excited into an unstable state from which they return to their original state with the release of blue light. By detection of this light, an image of the activity distribution in the sample can be built.

Compared to film, there are both advantages and disadvantages with phosphor screen technology. The most important advantages are the much longer linear range (4-5 orders of magnitude) and the higher sensitivity. With ^{32}P , the sensitivity has been reported to be 250 times higher than with film, and 60-100 times higher with ^{14}C and ^{35}S (Johnston et al 1990).

The higher sensitivity allows for shorter measuring times while the longer linear range reduces the risk of under exposure or over exposure.

Compared to film, the geometrical resolution obtainable is not equally good. With film and with a given nuclide, the resolution is dependent of the distance between the emulsion and the sample, and on the emulsion itself. In other words, it only depends on the process of energy deposition. With phosphor screen imaging, the resolution also depends on the scanning system, for example the laser spot size.

Another disadvantage is the need for careful handling of the plates. Before exposure, the plates have to be erased with light to remove records of previous exposures. Furthermore, the plates have to be cleaned properly. Finally, there is the signal fading, the process of the electrons returning to the ground state without stimulation with laser.

2.2.3 Digital Instruments for Autoradiography

With film, it is possible to obtain quantitative results by digitising an analogue image, and with phosphor imaging systems, digital images are obtained in the scanning process. In both cases, an analogue image with limited linearity is digitised. With digital autoradiography, nuclear transitions are counted one by one. This means that such systems features perfect linearity. Furthermore, as the hits are detected by an electronic system, the cumulative images are available at any time, and the need for accurate estimates of exposure times is thus eliminated.

Several digital systems for autoradiography exist which employ widely different detection principles (Charpak and Sauli 1978, Bateman et al 1985, Ljunggren and Strand 1990, Barthe et al 1999). Examples are proportional multiwire detectors and silicon strip detectors. Both principles were originally developed for high energy physics, but have found applications in autoradiography.

The instrument used in papers 3 and 4 is a silicon strip detector. A complete description of the principles used for particle detection in this instrument is outside the scope of this thesis. For a detailed description of semiconductor detectors, refer to Leo (1994). A brief description is given in paper 3.

One of the strengths of this apparatus is its capability of recording the energy deposited in each hit. This gives us the possibility of separating the signals from two different radionuclides with different particle spectra. Paper 3 shows how this can be done even with β -emitters that have overlapping energy spectra. The perfect linearity of digital instruments also permits a separation of radionuclides using differences in half-lives. This is only possible with

very good linearity. In paper 4, this is exploited for a comparison of the distributions of ^{153}Sm -EDTMP and ^{89}Sr in normal tissues, osteosarcoma, and metastases.

One important disadvantage with a silicon strip detector is that the geometrical resolution is poor with energetic β -particles. In the particular instrument used in paper 3 and 4, the detector has a thickness of $300\mu\text{m}$. If the particle hits the detector with a large entrance angle (relative to a perpendicular hit), the particle may travel a considerable distance before it comes to rest or reaches the opposite side.

For a characterisation of a radiopharmaceutical as a compound with certain chemical properties, it may be of interest to learn about the uptake pattern at a very detailed level. In a dosimetric perspective, it is not of much interest to investigate details of the uptake pattern that have dimensions much smaller than the range of the particles. This means that, although the FWHM increases with an increasing range in the detector, the measurements may be useful.

With nuclides that emit very short-ranged particles, the geometrical resolution is limited by the pixel dimensions. The pixels in the instrument used in paper 3 and 4 have sidelengths of $50\mu\text{m}$, and this instrument cannot compete with film for nuclides like ^3H . For the detailed dosimetry with very short particles, this silicon strip detector cannot be used.

Another problem encountered with the actual silicon strip detector, is the limited area of the detector. It is technically very difficult to make large area detectors, as the probability of getting one or more dead strips is increased. Also, the amount of electronics is increased. In paper 4, the problem of a small area is dealt with by cutting a section into smaller parts. After the imaging, the resulting sub images are merged to form one image of the whole section.

3 Methods for Dose Calculations

3.1 Definitions

It is of crucial importance to be aware that deposition of radiative energy is a stochastic process. The energy is mediated by particles (photons, electrons, or positrons) that travel in an unpredictable way. The quantum mechanical description of the processes that take place is a theory formulated in terms of probabilities. Anything that happens to a particle takes place with a certain probability. It is not possible to say for sure that this particle will end up at a certain position and undergo a given set of interactions. For this reason, it is necessary to define *stochastic* variables.

Absorbed energy, \mathcal{E} , is the amount of energy that is absorbed within some volume with the mass m . Specific energy is defined by (Rossi and Zaider 1996)

$$z \equiv \frac{\mathcal{E}}{m}. \quad (3.1)$$

This definition may resemble that of *dose*. However, specific energy is a stochastic variable, which furthermore depends on the shape and size of the volume. Dose is defined as the expectation value of z in the limit of an infinitesimally small volume (mass), and is a deterministic quantity (Rossi and Zaider 1996):

$$D \equiv \lim_{m \rightarrow 0} \bar{z}. \quad (3.2)$$

3.2 MIRD Formulation

In a clinical situation, it is important to be able to calculate doses without being an expert on radiation physics. For this reason, the Medical Internal Radiation Dose (MIRD) Committee has developed a simple system, which relates the mean dose in a target organ to accumulated activities in source organs (Loevinger et al 1988).

A certain radioisotope may emit several types of particles with different energies: Photons, electrons, positrons, and alpha-particles. For radiation type i , let the mean number of particles emitted per transition be denoted by n_i , and the particles energy by E_i . With a given source organ h , a mean fraction $\phi_i(k \leftarrow h)$ of E_i will be deposited in target organ k . For radiation type i , the mean energy deposited per transition will be equal to

$$n_i E_i \phi_i(k \leftarrow h). \quad (3.3)$$

If this quantity is divided by the target organs mass, the result is the mean dose in organ k delivered per transition in source organ h by radiation type i :

$$S_i(k \leftarrow h) = n_i E_i \phi_i(k \leftarrow h) / m \quad (3.4)$$

Summing over all radiation types gives the total dose per transition:

$$S(k \leftarrow h) = \sum_i S_i(k \leftarrow h). \quad (3.5)$$

These S-values have been calculated for all organ pairs and radionuclides that are of interest, and can be found in published tables. The information that must be obtained to find the dose in organ k delivered by organ h , is the cumulated activity defined by

$$\tilde{A}_h = \int_0^{\infty} A_h(t) dt, \quad (3.6)$$

where $A(t)$ is the activity at time t . In words, the cumulated activity is the total number of nuclear decays. The mean dose is now given by

$$\bar{D}(k \leftarrow h) = S(k \leftarrow h) \tilde{A}_h, \quad (3.7)$$

and the total mean dose delivered by all source organs is given by

$$\bar{D}_k = \sum_h \bar{D}(k \leftarrow h). \quad (3.8)$$

Evidently, the difficult part in applying this scheme is to determine the cumulative activity. In principle, it demands that the activity in each source organ is measured continuously over a time period of infinite length. However, in many situations, it is possible to adapt some mathematical model to describe the amount of activity as a function of time.

In the case of a radiopharmaceuticum that binds very strongly to some organ, it suffices to measure the activity that has been accumulated in this organ, A_{mi} . With an assumption of a very rapid uptake, the cumulated activity will then be given as

$$\tilde{A} = \int_0^{\infty} A_{mi} e^{-\frac{t \ln 2}{T_{1/2}}} dt = A_{mi} T_{1/2} / \ln 2, \quad (3.9)$$

where $T_{1/2}$ is the physical half-life of the nuclide.

S-values have also been calculated for single cells (Goddu et al 1997). This is applicable for microscopic disease with single cancer cells that is treated with a radioactive targeting compound. The radionuclides may be deposited in the cell nucleus, in the cytoplasm, or on the cell surface, and likewise, the target may be any of these compartments.

The published S-values for various organs are calculated using computational models. In these models, all the organs are described in terms of mathematically defined geometrical

objects with specific shapes and dimensions (ICRU 1992). The resulting S-values are obviously only correct for these idealized persons. In real life, the anatomical shapes and structures differ considerably between individuals, even of the same age and sex. Furthermore, some assumption has to be made about the distributions of the radionuclides within the source organs. For these reasons, the MIRD formalism can only supply information of limited accuracy.

3.3 Calculations with Dose Point Kernels

The increasing accuracy of the PET- and SPECT cameras opens up new possibilities for accurate dosimetry (Bolch et al 1999). For this purpose, the conventional MIRD formalism is not adequate, as only mean doses and uniform activity distributions are considered. With the easily available computer resources of today, more detailed calculations can be done using *Dose Point Kernels (DPK)* (Bolch et al 1999, Giap et al 1995).

A DPK is the mathematical description of the dose distribution resulting from a point source of unit activity. With the source centred in the origin, the value of the DPK at position (x,y,z) is the dose delivered to this point by the point source. It follows that the dose at a certain point is given as the convolution between the activity distribution and the DPK:

$$D(x, y, z) = \int_{\mathcal{V}} A(x', y', z') DPK(x - x', y - y', z - z') dx' dy' dz' = A(x, y, z) \otimes DPK(x, y, z) \quad (3.10)$$

For computations with a computer, it is natural to cast the description in the form of a 3D matrix, and the convolution is accomplished by a summation:

$$D(a, b, c) = \sum_{a'} \sum_{b'} \sum_{c'} A(a', b', c') DPK(a - a', b - b', c - c') \quad (3.11)$$

The shortcoming of this simple and powerful method is its inability to deal with volumes containing tissues of different densities (Bolch et al 1999). Examples from the human body are the boundary regions between lung tissue and air, and the complex problem of trabecular bone containing thin bone structures separated by bone marrow.

3.4 Monte Carlo Simulations

The physics of the interactions between radiation and matter is described by rather complicated probability density functions (pdfs). Furthermore, as interactions take place, particles are absorbed and created, and all in all, it is impossible to combine the pdfs of each

type of interaction in such a way that all possibilities are included. The only general and reliable method for calculations on radiation, is the Monte Carlo method.

Monte Carlo simulation is a numerical method that has become useful as computer resources became available. As the name suggests, it is a method where the calculated variables are dependent on random events, and more specifically, they are functions of a sequence of random numbers. This implies that the method returns stochastic variables, a unique feature of this method.

The method of Monte Carlo simulation is applicable for situations where the problem can be described in terms of one or more pdfs. The solutions to such problems are usually an integral over parts of the sample space. If there exist no analytical expression for the pdfs, or the number of dimensions is high, application of other numerical calculations may be difficult, or the time of computation may be very long. Another pleasant feature is the inherent simplicity of this method. Instead of analysing the problem in question as a whole, one can decompose it into smaller parts for which the pdfs are known.

The scheme for radiation transport is briefly as follows: Particles are generated according to some assumption about the source, where the source could be e.g. a linear accelerator or some spatial distribution of radioactive isotopes. Then each particle's trajectory is simulated according to the physics that is implemented in the code. Along its path, the particle undergoes interactions with the matter it traverses and the particle may change direction, lose energy, be absorbed, or new particles may be created. The particles that are created may be subject to their own individual simulation process, or their energy may be deposited locally as an approximation.

Today, several computer codes exist for simulation of radiation. Examples are EGS and ITS for coupled electron/gamma transport and MCNP for neutron/gamma transport. EGS was used for the Monte Carlo simulations performed in paper 2.

The backbone of any Monte Carlo code is the *random number generator* (RNG). Any event that takes place is a function of one or more random numbers. It is obvious that a number that is returned by a computer is not really *random*. However, one tries to generate sequences of numbers that passes several tests for randomness.

3.4.1 EGS

EGS (Nelson et al 1985) was originally developed for high energy physics at SLAC (Stanford Linear Accelerator Center), and it was only capable of handling particles in one

medium in one region. Over the years, it has been extended and modified to give reliable results also at low energies, and for complex geometries containing many different media.

For microdosimetric calculations with β -particles, some of the most important improvements are connected to electron transport. With electrons, an extremely high number of interactions take place along their path (of the order of 10^4 when slowing an electron from 0.5MeV to 1keV). It is unrealistic to simulate all these interactions, and for this reason, the *condensed history* techniques were developed. The strategy of these methods is to treat a group of consecutive interactions as one interaction by means of pdfs that describe the combined effects of multiple interactions.

As this code was intended for high-energy simulation, it was decided to use Molière's scattering theory. This is a theory for small angle scattering, i.e. the number of interactions that is grouped must be limited. This is equivalent to an upper limit on the step-size, the path length an electron is transported in each step in the simulation. With the small cross sections for large scattering angles at high energies, it was applicable for the tasks that EGS was originally meant for. Its validity is also limited downwards to a minimum step-size corresponding to a certain number of interactions.

In early versions of EGS, there were large problems with step-size artefacts, which are characterised as the dependence of some result upon the step-size of the electrons. If the result depends upon the step-size, some basic underlying constraint on the applied theories must be violated. This problem was a result of inadequate path length corrections, ignorance of lateral displacements and energy loss during a step, and non-accurate boundary crossing algorithms. All of these issues are related to the non-linear paths of electrons. (The path length correction is a correction to the distance that the electron travels along its original direction in one step. Lateral displacement is the movement perpendicularly on the original direction.)

As a remedy for these shortcomings of the code, several ad-hoc algorithms were introduced that were controlled by parameters which had to be set by the user for each physical situation that was to be simulated. A good code should work properly without having to do thorough tuning of such parameters.

The inclusion of PRESTA (Parameter Reduced Electron-Step Transport Algorithm) (Bielajew and Rogers 1987) very much eliminated these problems, and the number of parameters were reduced. However, there were still signs of step-size artefacts, especially in results depending on backscattering, and the step-size was still controlled by a parameter set by the user.

In the latest version of EGS called EGSnrc (Kawrakow 2000a,b), several substantial changes were made. Some of the most important were a new any-angle scattering theory, an improved electron-step algorithm, a more accurate evaluation of energy loss, and an exact boundary crossing algorithm. Simulation of ion chamber response and calculations of backscattered energy have been considered as the most stringent tests of electron transport simulation. It has been shown that EGSnrc give results that are within 0.1% of the theoretically known results for these situations. This version of EGS was used for the simulations in Paper 2.

The EGS code itself consists of a number of subroutines that must be called through a main program that is written by the user. Coding of the geometry, containing the different media, is accomplished through two subroutines called HOW-NEAR and HOW-FAR, which are also supplied by the user. HOW-FAR checks how far a particle can travel in its present direction before hitting a boundary. HOW-NEAR returns the distance to the nearest surface in any direction. Finally, the recording of the wanted results is done in another user-supplied subroutine.

In addition to the reliability of the results obtained with EGSnrc, the organisation of the program package gives other attractive properties. Compared to other codes, the EGS code system is very open and flexible. This demands more from the user, but it makes it a versatile tool for any imaginable situation.

3.5 Radiobiological Models

Radiobiological models are needed to be able to translate a calculated dose into biological effects. The model that is most frequently used, and the only one that will be presented here, is the linear-quadratic model. It was derived by Chadwick and Leenhouts (1973) on the basis of a few simple postulates regarding cell kill through the damages in the DNA, and the mechanisms leading to these damages. Briefly, their philosophy is that the critical damage is a double strand break, and that these may be created directly or as a combination of two single strand breaks.

Their final result is the following equation for the probability of cell survival:

$$S = e^{-(\alpha D + \beta D^2)}. \quad (3.12)$$

D is the dose to the cell nucleus, and α and β are constants that are specific to the cell type and the type of radiation (quality and energy). The first term in the exponent reflects cell kill

by direct double strand breaks, while the second term accounts for the combination of two single strand breaks.

Matters are complicated by a cell's ability to repair sublethal damages, i.e. single strand breaks that could have become part of a double strand break. If the dose is delivered in more than one fraction, or the dose rate is low, this is important with low LET irradiation. With fractionated radiation, eq. 3.12 is modified to

$$S = \prod_i e^{-(\alpha d_i + \beta d_i^2)}, \quad (3.13)$$

where d_i is the dose in fraction i . This equation is only valid with high dose rates, and with sufficiently long pauses between fractions for repair processes to complete. With unfractionated, low dose rate irradiation, the second term in eq. 3.12 is reduced by a factor g given by

$$g = 2(\mu t - 1 + e^{-\mu t}) / (\mu t)^2 \quad (3.14)$$

where $\mu = \ln 2 / T_{1/2}$ and $T_{1/2}$ is the repair half-time. For a derivation of eq. 3.14, the corresponding factor for fractionated irradiation with incomplete repair, and the factor for fractionated low dose rate irradiation, refer to Thames (1985) and Nilsson et al (1990).

3.5.1 Is the Mean Dose a Useful Quantity?

An organ in the human body consists of a vast number of cells which work together to perform certain tasks. The performance of the organ depends on how many of these cells are killed during the irradiation, and on their organisation within the organ.

Existing models for cell kill, with the linear-quadratic model as the most commonly used, are all formulated in terms of a probability that is a function of dose to the cell nucleus. None of these models makes use of the organ dose. Very often, the organ dose is the only available information, and the question is thus how to relate the organ dose to biological endpoints of the organ.

An organ may be classified by its inner organisation with serial organisation and parallel organisation as the extreme cases (Wolbarst et al 1982). A serial organ consists of modules that are connected in series, and the organ will not function if only one of these is malfunctioning. In a parallel organ, the modules are working in parallel, and the performance of the organ is proportional to the number of modules functioning.

Independent of the inner organisation, it is obvious that the biological effect of irradiation is not only dependent on the mean dose, but also on its spatial variation. This is

especially the case for tumours. In principle, one surviving tumour cell may be enough to give a relapse, and it is therefore of crucial importance to be able to irradiate all the tumour cells.

To illustrate the differences in the response of non homogeneous dose distributions, assume that each module receives a homogeneous dose equal to D_i . Then, in a serially organised organ the probability of retaining functionality will be given by

$$P_{mal}^{serial} = \prod_i e^{-(\alpha D_i + \beta D_i^2)}, \quad (3.15)$$

while for an organ with parallel organisation, the performance is proportional to

$$P_{perf}^{parallel} = \sum_i e^{-(\alpha D_i + \beta D_i^2)} \quad (3.16)$$

The partial derivatives of these expressions are

$$\frac{\partial P_{mal}^{serial}}{\partial D_i} = -P_{mal}^{serial} (\alpha + 2\beta D_i) \quad (3.17)$$

and

$$\frac{\partial P_{perf}^{parallel}}{\partial D_i} = -e^{-(\alpha D_i + \beta D_i^2)} (\alpha + 2\beta D_i). \quad (3.18)$$

This shows that for a serially organised organ, it is the maximum doses that are most important. For the organs with parallel organisation, a reduction in the dose to the parts of the organ that receives the lower doses has a greater positive effect on the performance of the organ than a reduction in the maximum doses.

3.6 An Illustration of the Dose Point Kernel Method and Monte Carlo Simulation

There has been much discussion about the preferred characteristics of a radionuclide. Several factors are important: the range of the emitted particles, the half-life, the chemical properties, and availability. With homogeneity in dose deposition within a tumour as one goal, it is rather easy to explore the consequences of the first of these properties, the range.

As part of this dissertation, the following investigation was carried out. Suppose we have a promising new targeting agent and want to find the best radionuclide to attach to this molecule. We limit ourselves to the radionuclides ^{90}Y , ^{153}Sm and ^{131}I . For solid tumours with diameter $2R$, it has been found that the uptake of the radiopharmaceutical varies according to

$$A(r) = ae^{-b(R-r)} \quad (3.19)$$

where r is the distance from the centre of the tumour, R is the radius of the tumour, and a and b are constants with $b=0.5\text{cm}$. The aim of this limited investigation is to find the dose distributions in spherical tumours with R equal to 0.2, 0.5, 1.0 and 2.0 cm.

Assume that external sources can be neglected. Then the problem can be solved by convolution between a Dose Point Kernel (DPK) and the activity distribution. As a first step, the DPK has to be found by means of Monte Carlo simulation. The results of these simulations are shown in figure 3.1.

In the simulations, particles are “born” at the origin according to the decay spectrum of the specific nuclide. Because of the spherical symmetry of this specific problem, it is not necessary to spend CPU-time on generating random directions of travel, and all the particles are initially travelling in the same direction.

Space is divided into concentric spherical shells around the origin, and as the particles move outwards from the origin, the energy depositions are assigned to these shells. For each nuclide, 100 000 decays are simulated. The total energy deposited in each shell is divided by the number of decays and the volume of the shell to give the dose. With very thin shells, a quasi-continuous dose distribution is obtained.

To be able to carry out the convolution with the activity contribution given by eq. 3.19, both the DPK and the activity distribution must be represented by matrixes. Finally, the convolution may be performed.

Because of the spherical symmetry, it suffices to calculate the dose distribution along a given line through the origin. Furthermore, it is only necessary to do the convolution with a quarter of the DPK, and then multiply the result by four. Even so, the geometrical resolution of the matrixes of the DPK and the activity distribution is limited by CPU-capacity and the available amounts of memory. The results of the convolutions are shown in figure 3.2.

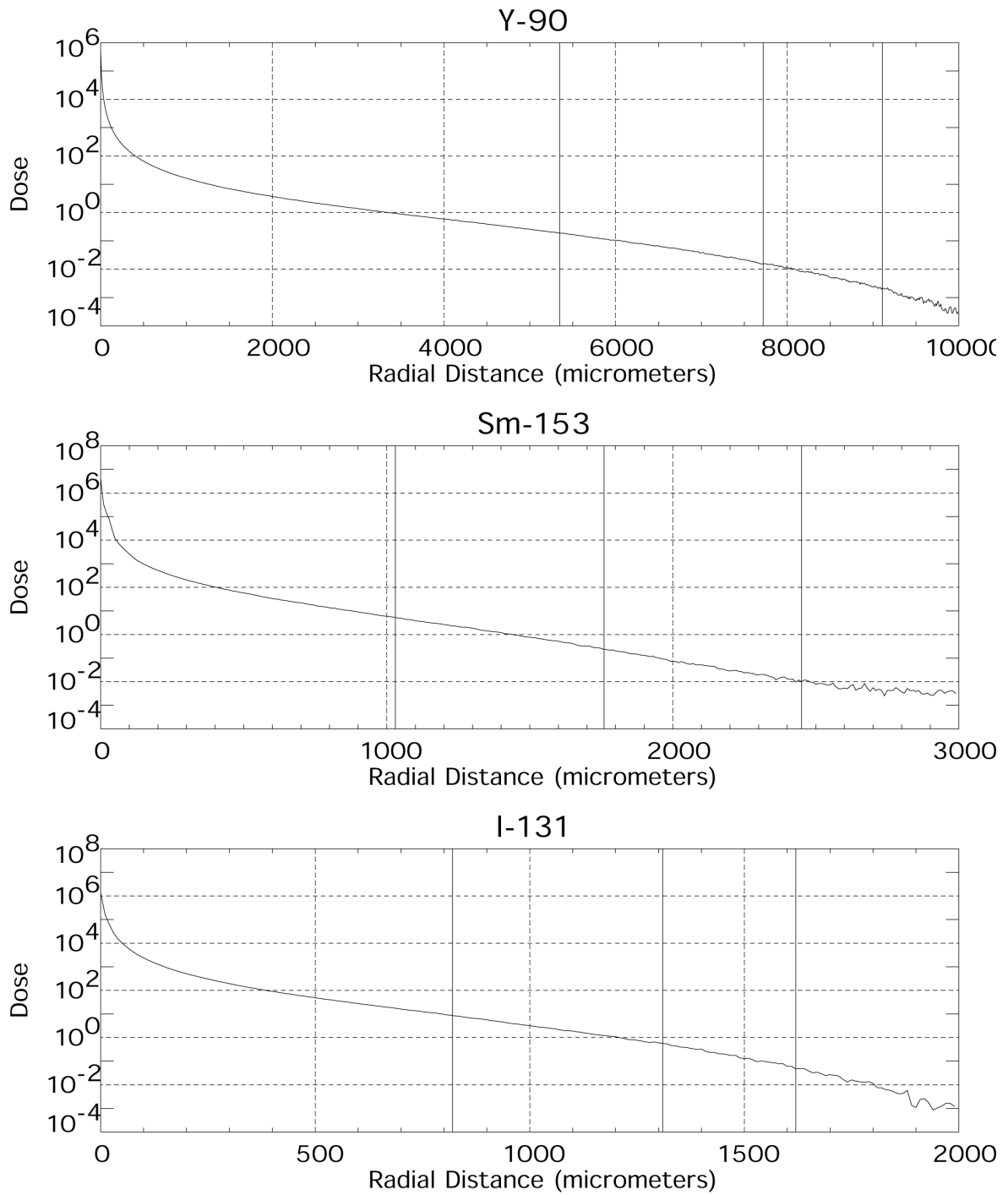


Figure 3.1 Dose per decay around point sources. Dose is in units of MeV/cm^3 . Vertical solid lines indicate the radii of the spheres containing 90%, 99% and 99,9% of the energy. (Unpublished data).

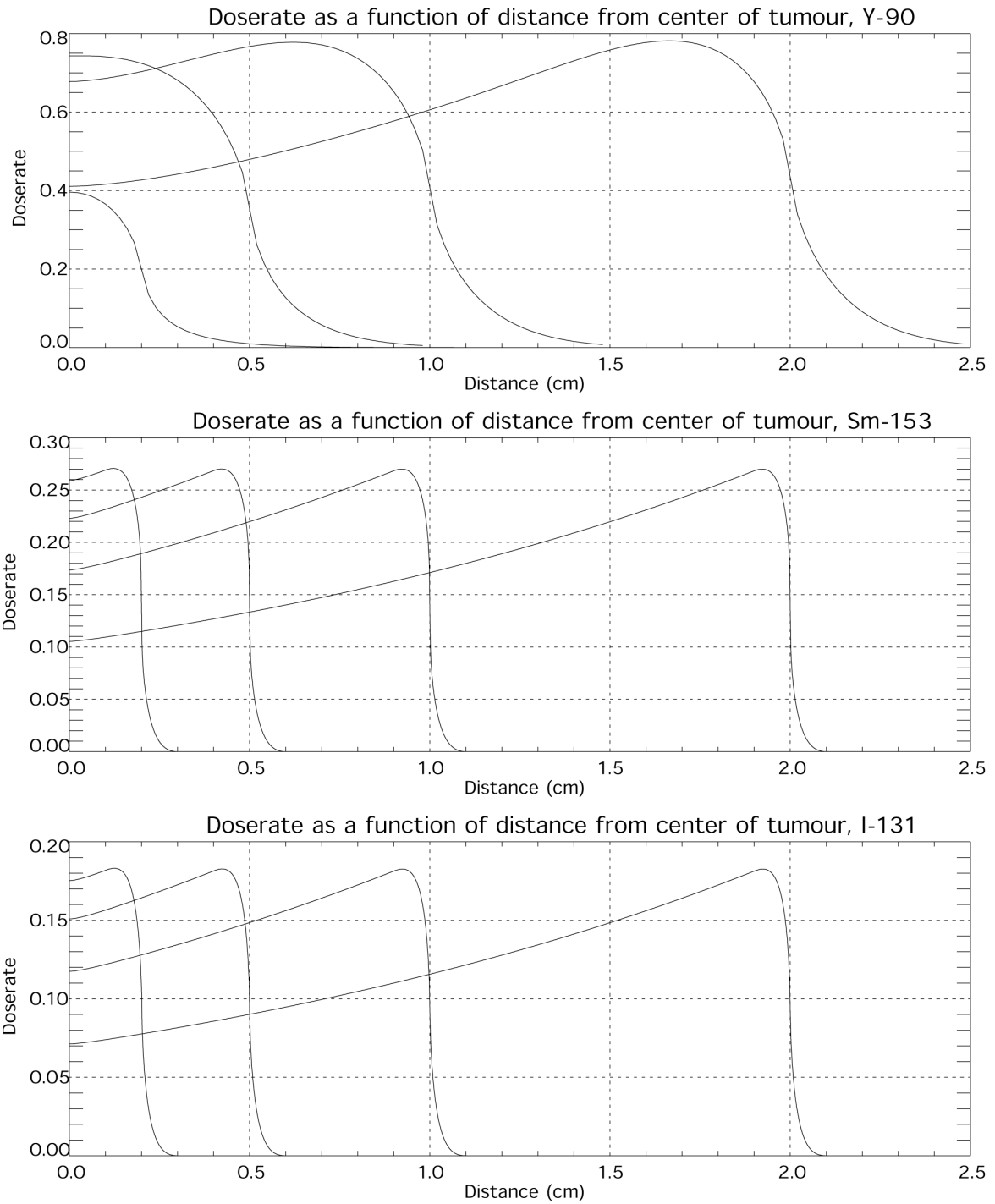


Figure 3.2 Dose rate as a function of radial distance. The constant a of equation 3.19 is set equal to 1 Bq/cm³. The dose rate is in units of MeV/cm³.s. (Unpublished data).

The figure clearly shows some of the advantages and disadvantages of the nuclides. The long range of the ⁹⁰Y β -particles ensures that the centre regions of the tumours, where the activity is low, receives a quite high dose. With the largest tumours (radius of 2 cm), the dose in the origin is slightly higher than half of the maximum dose with ⁹⁰Y, while it is

approximately 2.5 times lower with the two other nuclides. In the smallest of the tumours (radius of 0.2 cm), the maximum dose is actually located at the origin with ^{90}Y .

At the edges of the tumours, the dose is of course only approximately half of the maximum dose for all the tumours and nuclides. However, the volume in the outer parts of the tumours that receives considerably lower doses than the maximum dose, is much larger with ^{90}Y than with the other nuclides. Correspondingly, the doses outside the tumours are high with ^{90}Y .

A similar study has been performed by Nahum (1996). Using an assumption of a perfectly homogeneous activity distribution, this author calculated dose distributions for six different β -emitters, and from the data obtained, tumour control probabilities (TCP) that were compared with corresponding results with external beam radiotherapy. For a more complete discussion of dosimetry of solid tumours, see Meredith et al (1993).

One possible approach to obtain an effective treatment that spares the normal tissue, is a cocktail containing a mixture of the different radionuclides. The amounts of nuclides with short and long ranges could be adjusted to the anticipated distribution of radii in the metastases, and to the radiation sensitivity of the normal tissues surrounding these.

4 Dosimetry in Trabecular Bones

For dosimetric purposes, the tissues of the human body can be divided into two categories: soft tissues and bone. Variations in the densities of soft tissue are negligible in most cases. Bone has a density of nearly twice that of soft tissues, 1.9g/cm^3 vs. 1.0g/cm^3 (ICRU 1989).

Dosimetry in volumes containing only one of these two types of tissue is rather simple. With a known activity distribution, the dose distribution is obtained by a convolution with the DPK of the nuclide in question. The difficulties arise when the volumes of interest contain media of different densities. In that case, the only reliable and general method is the Monte Carlo method.

The structure of the human body that presents the most difficult dosimetric situation is the trabecular bones (cancellous bones). As an incidence of bad luck, they furthermore contain the very important, and radiosensitive, bone marrow, where blood cells are produced (Cristy 1981). For all kinds of treatments with unsealed internal radionuclides, the red marrow is the dose limiting tissue (Lewington 1996). For these reasons, it has been considered very important to be able to calculate doses to this tissue, and to the cells that constitute the lining of the inorganic bone masses, the endosteal layers.

4.1 The structure of trabecular bone.

Trabecular bone tissue is found at the ends of long bones, in flat bones, and in the vertebrae. It resides in the interior of bones, surrounded by solid cortical bone. As illustrated in fig. 4.1, it consists of an intricate network of thin bone columns and plates with marrow cavities in between (Singh 1978). The structure adds considerable additional strength to the skeleton with only a small increase in bone mass (Jensen and Mosekilde 1990).

Although irregular in its structure, it is possible to identify differences between various sites in the skeleton. The orientations of the bone trabeculae are isotropically distributed in bone that carry no weight, such as the ribs, while they are oriented parallel or perpendicular to the directions of load in for instance the vertebrae (Turner 1992). Furthermore, the dimensions of the cavities and the trabeculae also vary between different sites in the skeleton (Beddoe et al 1976).

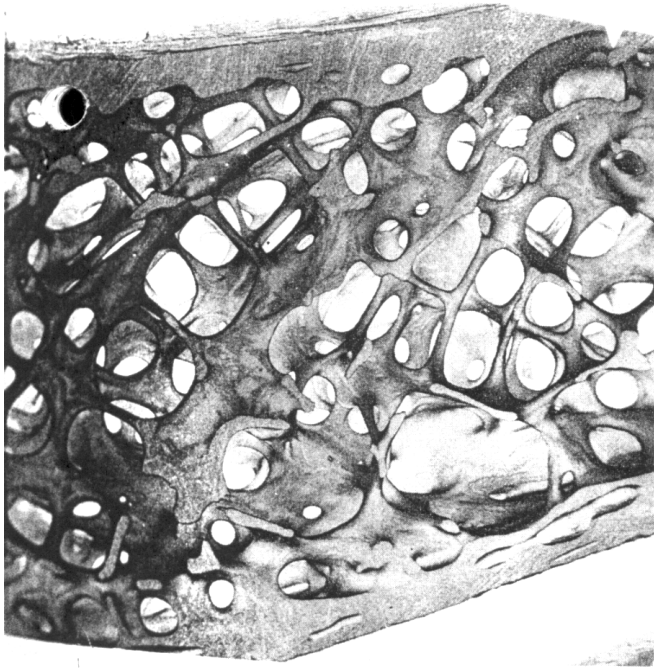


Figure 4.1 A sample of trabecular bone.

The bone marrow is located in the cavities that separate the trabeculae. The bone marrow can be either haematopoietically active (red), or it can be inactive (yellow). The marrow is separated from the inorganic bone masses by the endosteum, a thin layer of cells. This layer houses the osteoblasts and the osteoclasts.

The osteoblasts are responsible for the bone formation. They secrete the organic component of the bone matrix, and they are responsible for the inclusion of extracellular inorganic calcium salts. After finishing the bone formation, osteoblasts are converted to osteocytes. The majority of these remain at the bone surfaces as lining cells, while about every 10th osteocyte is incorporated into the newly formed osteoid. The osteoclasts are the bone removers. They are active in areas where bones change in shape (Mosekilde 1989).

The dosimetrically important cells in trabecular bone are the osteoblasts, the osteoclasts, and the haematopoietic stem and precursor cells. With high doses, total ablation of the red marrow may become the result, and bone marrow transplantation is necessary to rescue the patient. From the viewpoint of radiation protection, these are all cells that may transform into cancer cells. Mutations in the bone cells, osteoblasts and osteoclasts, may lead to osteosarcoma, while damages in the blood cells' DNA may lead to leukaemia.

4.2 Calculations of Dose in Trabecular Bone

Fig. 4.1 clearly shows that the structure of trabecular bones is not regular and composed of many repetitive equal unit elements. It was early recognised that it is impossible to give a geometrical description of it in terms of mathematically well-defined objects. For this reason, a group at the University of Leeds (Beddoe et al 1976) designed an optical bone scanner that was capable of measuring cord lengths in trabeculae and bone marrow spaces.

The apparatus consisted of a laser that was directed towards a detector. A thin section of trabecular bone was positioned between the detector and the laser. When slowly moving this section over the light source, the light would reach the sensor through the marrow cavities while it was stopped by the bone trabeculae. By measuring the length of time when the light hit the sensor and the periods when it didn't hit the sensor, cord lengths were obtained.

Cord length distributions were measured for seven different sites in the skeleton: Parietal bone, cervical vertebra, lumbar vertebra, rib, iliac crest, femur head, and femur neck. These measurements showed that there are large differences in the trabecular structures at the various skeletal locations. Fig. 4.2 shows the cord length distributions for trabecular bone in a lumbar vertebrae.

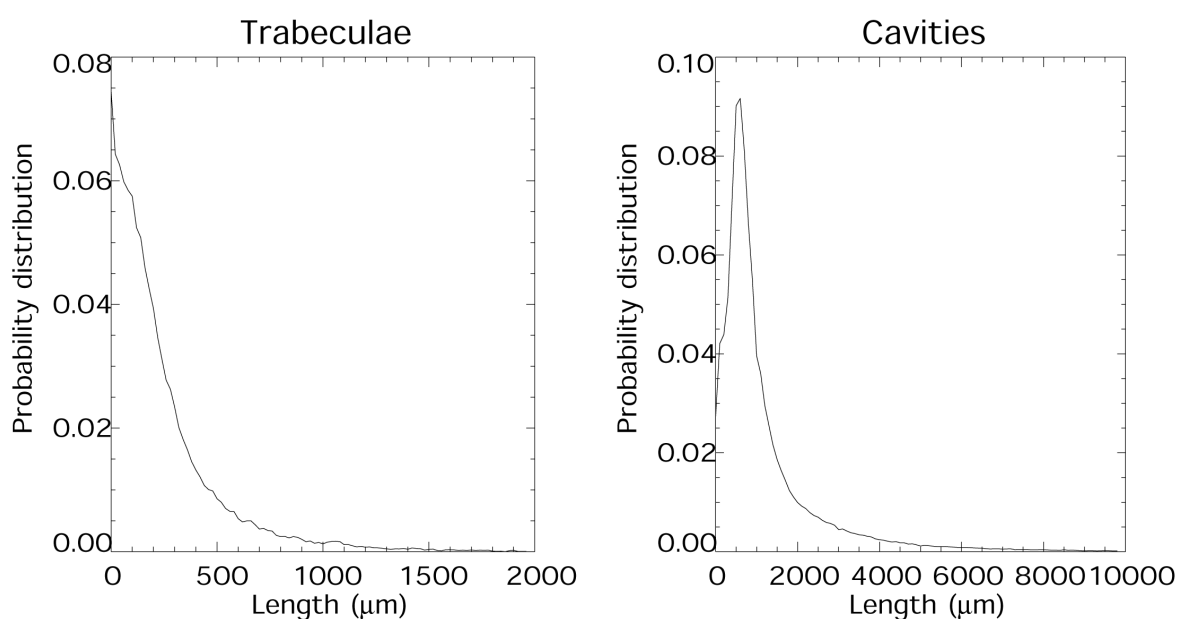


Figure 4.2 Cord length distributions for a lumbar vertebrae.

Whitwell and Spiers (Whitwell 1973, Whitwell and Spiers 1976, Spiers et al 1978a, Spiers et al 1978b, Spiers et al 1981) used these distributions to calculate dose conversion factors for nuclides of interest in health physics. Later, Eckerman (1985) calculated absorbed

fractions of energy for monoenergetic electrons. By assuming that the electrons travelled through the cavities/trabeculae in straight lines, the problem could be reduced to a 1-dimensional Monte Carlo problem: Depending on the source configuration, i.e. which tissue contained the radioactive nuclides, the first path length was chosen from the appropriate cord length distribution. The electron was assumed to travel this length, and the energy loss of the electron was calculated and assigned to the actual medium. Then a new cord length was sampled from the other cord length distribution, and the process was repeated. This procedure went on until the electron had lost all its energy. By repeating this algorithm for a high number of electrons, a mean deposited energy could be calculated for the different tissues.

Despite its simplicity and obvious approximations, the development of this method was a breakthrough in dosimetry in trabecular bones. Earlier, it had been considered an intractable problem to find absorbed fractions of energy in this complicated structure. Snyder et al (1975) converted Whitwells (Whitwell 1973) results into S-values for mono-energetic electrons using the mean β -particle energy, and they were used in MIRD pamphlet no. 1. Eckermans results were included in the computer code MIRDOSE 3 (Stabin 1996), intended for use in nuclear medicine. In the work by Eckerman and Stabin (2000), this method is used to find absorbed fractions of energy for electrons in various skeletal regions for individuals of different age, and the results were weighted to give average skeletal absorbed fractions.

The accuracy of this model is limited by the non-linearity of the electron paths, and the production of bremsstrahlung photons and delta rays (Kwok et al 1991, Johnson et al 1992). To be able to include these effects, 3-dimensional Monte Carlo simulations are necessary. However, this requires a 3-dimensional geometrical description of the marrow cavities and trabeculae.

In the work by Bouchet et al (1999), also conducted to find mean doses to tissues in trabecular bone, it was realised that one can avoid the construction of an accurate geometrical model of the entire bone by concentrating on the geometry that the electron will see before it comes to rest. For each time the electron leaves one medium, it is allowed to enter a hemisphere for which the radius is calculated from a cord length that is sampled from the measured cord length contributions. The electron enters the hemisphere through the planar side of the hemisphere, and the effect of backscattering is taken into account whenever an electrons reverses its direction of travel and leaves the hemisphere through this plane. When secondary particles are produced, these are treated as independent particles.

Jokisch et al (1998, 2001a, 2001b) investigated the applicability of NMR to obtain structural data for dosimetry. The data was used in two ways: To obtain cord length

distributions analogous to those collected by Spiers and co-workers, and to perform Monte Carlo simulations with a trabecular bone described in terms of voxels.

The cord length distributions obtained with this method were in fairly good agreement with those obtained with optical scanners. However, the results indicated that the distributions for trabeculae and cavities are not statistically independent. The independence of these distributions was a fundamental assumption in the dose calculations used until this date, based on cord length distributions. It was furthermore shown that the doses calculated with voxel representation of the bones, were in close agreement with doses calculated using the model of Bouchet et al (1999) (calculated with cord length distributions acquired from NMR data from the same sample that was used for the voxel data).

All these previous methods are designed to return *mean* doses to the various tissues, bone marrow, endosteum, and the bone volume. It is obvious that applying the mean dose to calculate the fraction of surviving stem cells will in general not give the right answer. In principle, the dose has to be found for each cell nucleus along with the corresponding survival probability. This can be expressed mathematically by the following:

$$S = \int_V n(\vec{r})P(D(\vec{r}))dV \quad (4.1)$$

with $n(\vec{r})$ being the density of cells at position

ERROR: typecheck
OFFENDING COMMAND: makefont

STACK:

[49.844 0 0 -49.844 0 0]
5
false
/F5S31